http://informahealthcare.com/nan
ISSN: 1743-5390 (print), 1743-5404 (electronic)

Nanotoxicology

Nanotoxicology, 2014; 8(S1): 216–225
 DOI: 10.3109/17435390.2013.879612

informa
healthcare

ORIGINAL ARTICLE

Tracking translocation of industrially relevant engineered nanomaterials (ENMs) across alveolar epithelial monolayers *in vitro*

Joel M. Cohen[1], Raymond Derk[2], Liying Wang[2], John Godleski[1], Lester Kobzik[1], Joseph Brain[1], and Philip Demokritou[1]

[1]*Department of Environmental Health, Center for Nanotechnology and Nanotoxicology, Harvard School of Public Health, Boston, MA, USA and* [2]*Health Effects Laboratory Division, Pathology and Physiology Research Branch, National Institute for Occupational Safety and Health (NIOSH), Morgantown, WV, USA*

Abstract

Relatively little is known about the fate of industrially relevant engineered nanomaterials (ENMs) in the lungs that can be used to convert administered doses to delivered doses. Inhalation exposure and subsequent translocation of ENMs across the epithelial lining layer of the lung might contribute to clearance, toxic effects or both. To allow precise quantitation of translocation across lung epithelial cells, we developed a method for tracking industrially relevant metal oxide ENMs *in vitro* using neutron activation. The versatility and sensitivity of the proposed *in vitro* epithelial translocation (INVET) system was demonstrated using a variety of industry relevant ENMs including CeO_2 of various primary particle diameter, ZnO, and SiO2-coated CeO_2 and ZnO particles. ENMs were neutron activated, forming gamma emitting isotopes ^{141}Ce and ^{65}Zn, respectively. Calu-3 lung epithelial cells cultured to confluency on transwell inserts were exposed to neutron-activated ENM dispersions at sub-lethal doses to investigate the link between ENM properties and translocation potential. The effects of ENM exposure on monolayer integrity was monitored by various methods. ENM translocation across the cellular monolayer was assessed by gamma spectrometry following 2, 4 and 24 h of exposure. Our results demonstrate that ENMs translocated in small amounts (e.g. <0.01% of the delivered dose at 24 h), predominantly via transcellular pathways without compromising monolayer integrity or disrupting tight junctions. It was also demonstrated that the delivery of particles in suspension to cells in culture is proportional to translocation, emphasizing the importance of accurate dosimetry when comparing ENM–cellular interactions for large panels of materials. The reported INVET system for tracking industrially relevant ENMs while accounting for dosimetry can be a valuable tool for investigating nano–bio interactions in the future.

Keywords

Dosimetry, *in vitro*, nanotechnology, nanotoxicology, translocation

History

Received 29 October 2013
Revised 27 December 2013
Accepted 27 December 2013
Published online 30 January 2014

Introduction

The increasing manufacture and use of engineered nanomaterials (ENMs) in electronics, cosmetics, toner formulations, and biomedical applications, raises questions regarding their environmental and occupational health and safety (Aitken, 2006; Bello et al., 2012; Pirela et al., 2013). Human exposure via inhalation in particular is a growing concern. Studies have demonstrated inhaled ENMs can pass from the lungs into the bloodstream and enter extrapulmonary organs (Choi et al., 2010; Geiser et al., 2005; Kreyling et al., 2009), thereby increasing risk of cardiovascular morbidity and mortality (Brain et al., 2009; Mills et al., 2009). However, relatively little is known for industrially relevant ENMs regarding their fate, potential toxicity, and mechanisms of translocation in biological cells, tissues and organs (Kim et al., 2010; Yacobi et al., 2010).

Inhaled ENMs likely enter the systemic circulation across the alveolar epithelium, a very thin biological barrier (~0.5 μm) that constitutes >95% the surface area (~100 m^2 in humans) in distal airspaces of the lung (West, 2008). ENMs may translocate across the alveolar epithelium transcellularly via transcytosis (Conner & Schmid, 2003) and other non-endocytic mechanisms, or paracellularly via tight junctions. While hydrophilic solutes of hydrodynamic radius <6 nm have been reported to passively translocate via paracellular pathways by restricted diffusion (Kim & Crandall, 1983; Matsukawa et al., 1997), nanoparticles >10 nm in diameter are expected to be excluded from tight junctions under normal conditions (Yacobi et al., 2010). If, however, ENM exposure disrupts tight junctions and compromises the epithelial monolayer barrier, paracellular transport could be increased. The effect of specific ENM properties on translocation across the alveolar epithelium, and whether transport occurs via a predominantly transcellular or paracellular pathway is not well-understood. The mechanism and extent of ENM translocation across epithelial monolayers hold implications for ENM clearance from the lungs as well as pulmonary and cardiovascular toxicity.

One major challenge in performing such studies is employing tracer particle models for tracking industrially relevant ENMs. Most *in vitro* studies utilize fluorescently labeled polystyrene beads for tracking particle–cell interactions (Rothen-Rutishauser et al., 2005; Xia et al., 2008b; Yacobi et al., 2010). These

Correspondence: Philip Demokritou, Department of Environmental Health, Center for Nanotechnology and Nanotoxicology, Harvard School of Public Health, Boston, MA, USA. E-mail: pdemokri@hsph.harvard.edu

particles, however, are not representative of industrially relevant ENMs, are generated via wet-synthesis methods (Rothen-Rutishauser et al., 2005; Xia et al., 2008b; Yacobi et al., 2010; Yang et al., 2013), and there is low likelihood of inhalation exposure to these particles in aerosolized form. Furthermore, fluorescently labeled nanoparticles exhibit relatively low sensitivity for detecting small concentrations of particles, label instability, altered physicochemical properties such as surface chemistry and charge, and photobleaching from laser exposure (Nel et al., 2009; Sotiriou et al., 2012; Tenuta et al., 2011). Moreover, ENM transformations and agglomeration in liquid suspension and the subsequent effects on particle transport and delivery to cells in culture are often overlooked (Cohen et al., 2012; Deloid et al., 2013; Hinderliter et al., 2010; Teeguarden et al., 2007).

An optimal tracer particle model for ENM translocation studies should enable tracking of industrially relevant ENMs. One particular class of ENMs with many industrial uses is flame-generated metals and metal oxides. Flame-generated synthesis of ENMs is the currently preferred route by nanotechnology industry, and they account for the highest volume of ENMs in production (Wegner & Pratsinis, 2003).

We present here a novel *in vitro* method for tracking ENM translocation across Calu-3 human lung epithelial monolayers. The proposed system utilizes well-characterized industrially relevant metal oxide ENMs, using a neutron activation technique. This radiotracer technique is a well-established method that enables tracking of flame-generated metal oxide nanoparticles for biodistribution studies *in vivo*, but has yet to be used extensively for *in vitro* studies (Chen et al., 2010; He et al., 2010; Yeh et al., 2012; Wang et al., 2010). A number of industry relevant ENMs such as CeO_2 and ZnO nanoparticles were utilized in this study to show the versatility of the proposed method. Those ENMs were selected here due to their range in toxicity as well as their extensive presence in consumer products [including cosmetics, fuel additives, polishing slurries, etc. (Demokritou et al., 2013; Gass et al., 2013)]. We also included ''core shell'' composite ENMs, consisting of either a CeO_2 or ZnO core and a hermetic nano-thin coating of amorphous SiO_2 (Gass et al., 2013), in order to assess the effect of surface chemistry, particle size, and chemical composition on translocation across cellular monolayers.

Materials and methods

Nanomaterial synthesis and characterization

ENMs investigated are listed in Table 1. All ENMs were generated using the Harvard Versatile Engineered Nanomaterial Generation System (VENGES), as previously described (Demokritou et al., 2010, 2013; Gass et al., 2013; Sotiriou et al., 2011). ENMs were characterized for primary particle size and specific surface area. Specific surface area, SSA, defined as the area per mass (m^2/g), was determined by the nitrogen adsorption/Brunauer–Emmett–Teller (BET) method (Micromeritics TriStar, Norcross, GA). The equivalent primary particle diameter, d_{BET}, was calculated, assuming spherical particles, as:

$$d_{BET} = \frac{6}{SSA \times \rho_p} \quad (1)$$

where ρ_p is the particle density, which was obtained for each particle from the densities of component materials, at 20 °C, reported in the CRC handbook of Chemistry and Physics (Haynes, 2012). Primary particle diameter was also determined by X-ray diffraction using a Scintag XDS-2000 Powder Diffractometer (Cupertino, CA) [Cu K_α ($\lambda = 0.154$ nm), −40 kV, 40 mA, step size = 0.02°] following previously described methods (Gass et al., 2013), and reported as d_{XRD} (in nanometer). Particle morphology and size were further characterized by transmission electron microscopy (TEM) (Supplementary Figure 1) using a Libra 120 TEM (Zeiss, Oberkochen, Germany).

ENM dispersal and characterization in liquid suspensions

ENM dispersion was performed using a protocol previously described by the authors and included calibration of sonication equipment to ensure accurate application and reporting of delivered sonication energy (DSE) in Joule/milliliter, as well as determination of the material specific critical DSE (Cohen et al., 2012). ENMs were dispersed at 1 mg/ml in 10 ml of solute in 50 ml, conical polyethylene tubes, by sonication with a cup horn Branson Sonifier S-450 A (Branson Ultrasonics Corporation, Danbury, CT) (maximum power output of 400 W at 60 Hz, continuous mode, output level 3, power delivered to sample: 1.25 W). Dispersions were analyzed for hydrodynamic diameter (d_H), polydispersity index (*PdI*) and zeta potential (ζ) by dynamic light scattering (DLS) using a Zetasizer Nano-ZS (Malvern Instruments Ltd, Worcestershire, UK). Stock solutions prepared in deionized water (DI H_2O) were then diluted to desired concentrations (0, 6.25, 12.5, 25, 50 and 100 μg/ml) in cell culture media [Eagle's Minimum Essential Medium (MEM)/5% fetal bovine serum (FBS)] prior to characterization for various particle and media parameters, or application to cells for toxicological evaluation.

Suspensions were also characterized for agglomerate effective density by the Harvard volumetric centrifugation method recently developed by the authors, described elsewhere (Demokritou et al., 2012; Deloid et al., 2013). In brief, 1 ml

Table 1. Characterization of ENM powders and liquid suspensions.

Material	SSA (m^2/g)	d_{BET} (nm)	d_{XRD} (nm)	ρ (g/cm^3)	Media	d_H (nm)	ζ (mV)	ρ_E (g/cm^3)
CeO^2 – small					DI H^2O	136 ± 1.06	34.5 ± 3.15	NA
$d^{XRD} = 28.4$ nm	28.0	28.0*	28.4	7.65	MEM/5%FBS	184 ± 2.40	−12.5 ± 0.289	1.625
CeO^2 – large	11.0	71.9*	119	7.65	DI H^2O	231 ± 2.93	34.5 ± 3.15	NA
$d^{XRD} = 119$nm	31.3	29.2	28.4	6.29	MEM/5%FBS	215 ± 3.42	−9.77 ± 0.497	2.368
SiO^2-coated CeO^2	40.14	26.7	28.0	5.6	DI H^2O	208 ± 2.87	−26.8 ± 0.277	NA
$d^{XRD} = 28.4$ nm	66.0	18.5	27.6	4.13	MEM/5%FBS	227 ± 3.17	−11.6 ± 0.451	1.600
ZnO	11.0	71.9*	119	7.65	DI H^2O	218 ± 3.9	23.0 ± 0.462	NA
$d^{XRD} = 28.0$ nm	31.3	29.2	28.4	6.29	MEM/5%FBS	235 ± 2.55	−15.5 ± 3.29	1.485
SiO^2-coated ZnO					DI H^2O	165 ± 1.71	−15.9 ± 1.27	NA
$d^{XRD} = 27.6$ nm	40.14	26.7	28.0	5.6	MEM/5%FBS	206 ± 4.52	−12.6 ± 5.77	1.655

SSA: (specific surface area) by nitrogen adsorption/BET method; d_{BET}: particle diameter determined from SSA and particle density, ρ, as described in methods; d_{XRD}: particle diameter by X-ray diffraction; ρ: material density; d_H: hydrodynamic diameter; *PdI*: polydispersity index; ζ: zeta potential; ρ_E: agglomerate effective density.

*d_{BET} assumes spherical particles, CeO_2 particles are hexagonal so d_{XRD} is a more accurate description of primary particle size.

samples of 100 μg/ml suspensions of metal oxide ENMs were dispensed into TPP packed cell volume (PCV) tubes (Techno Plastic Products, Trasadingen, Switzerland) and centrifuged at 2000*g* for 1 h. Agglomerate pellet volumes, V_{pellet}, were measured and agglomerate densities were calculated from V_{pellet} values of triplicate samples for each ENM.

In vitro dosimetric considerations

The *in vitro* sedimentation, diffusion and dosimetry (ISDD) model proposed by Hinderliter et al. (2010) and described previously (Cohen et al., 2012) was used to calculate numerically for all ENMs studied, the fraction of administered particles that would be deposited onto cells as a function of time $f_D(t)$. The agglomerate hydrodynamic diameter, d_H, and the measured effective density were used as inputs to the model and are listed in Table 1. Additionally, the following parameters were used as inputs to the ISDD numerical model: media column height, 1.5 mm; temperature, 37 °C; media density, 1.00 g/ml; viscosity, 0.00074 Pas for MEM/5% FBS; and administered (initial suspension) particle concentration, 12.5 μg/ml (Hinderliter et al., 2010).

Neutron activation of industry relevant ENMs

ENM powders were irradiated with neutrons for up to 24 h at the Nuclear Reactor Laboratory (Massachusetts Institute of Technology, Cambridge, MA), and the radioactive ^{141}Ce ENMs (CeO_2, SiO_2-coated CeO_2) and ^{65}Zn ENMs (ZnO, SiO_2-coated ZnO) were stored in irradiation tubes. ^{141}Ce and ^{65}Zn are gamma emitters with a half-life of 32 and 244 days, respectively, and the successful production of radioactive ENMs following irradiation was confirmed by gamma energy spectrometry using a Packard Gamma Counter (Cobra Quantum; Packard Instruments, Downers Grove, IL). ENMs were quantified as either percentage of total administered mass dose, or percentage of the estimated delivered dose, based on total measured radioactivity (counts per minute, CPM). Concentration calibrations were performed for each ENM by measuring radioactivity for a measured and known total ENM mass in suspension, and measuring radioactivity of dilutions by half down to 5 ng.

Cell culture and cytotoxicity experiments

Immortalized human lung epithelial cells [CalU-3 (HTB-55); ATC Ingredients Inc, Manassas, VA] were cultured in MEM culture media supplemented with 5% heat inactivated FBS, 100 U/ml penicillin, 100 μg/ml streptomycin and 10 mM HEPES. Culture media components were obtained from Sigma Aldrich (St. Louis, MO). All incubations were performed at 37 °C/5% CO_2. Cellular metabolic activity and cytotoxicity were measured via the 3-(4,5-dimethylthiazol-2-yl)-2,5-diphenyltetrazolium bromide (MTT) and lactate dehydrogenase (LDH) assay, respectively according to the standard protocols previously reported (Demokritou et al., 2013; Gass et al., 2013). All experiments were conducted in triplicate for each ENM.

Absorbance values measured for LDH and MTT *in vitro* assays were normalized with negative control (particle-free media) and positive control (Triton X-100; Sigma Aldrich, St. Louis, MO) absorbance values, to a metric of cell viability (%) using the following equation:

$$\text{Cell viability}(\%) = \frac{\left\{\begin{array}{l}\text{Sample Absorbance}\\ \quad -\text{Negative Control Absorbance}\end{array}\right\}}{\left\{\begin{array}{l}\text{Positive Control Absorbance}\\ \quad -\text{Negative Control Absorbance}\end{array}\right\}}$$

Variance of toxicity results for each ENM was tested by *post hoc* one-way analysis of variance (ANOVA) with significance set at $p \leq 0.05$. One-tailed unpaired Student's t test was used for significance testing, with significance set at $p \leq 0.05$.

Monitoring of formation and barrier integrity of cellular monolayer

Several methods were used to monitor the formation and integrity of cellular monolayers and tight junctions. In more detail:

Transepithelial electrical resistance (TEER)

Calu-3 cells were seeded at 5×10^5 cells per well onto 6.5-mm Transwell® tissue culture-treated inserts (polyester membrane with 3.0 μm pores and 0.33 cm^2 growth area) with 100 μl of particle-free MEM/5% FBS in the apical region and 600 μl particle-free MEM/5% FBS in the basal region, and cultured at 37 °C in humidified air with 5% CO_2. Resistance of the cell monolayer within each well, reported in ohms per square cm of growth area ($\Omega\,cm^2$), was monitored daily prior to exposure using the Epithelial Voltohmmeter and STX2 electrode (World Precision Instruments, Sarasota, FL), and the resistance of filters without cells was subtracted from all sample measurements. Wells reporting resistance $>500\,\Omega\,cm^2$ were assumed to have achieved monolayers with tight junctions, supported by previous findings in the literature (Geys et al., 2006, 2007; Rothen-Rutishauser et al., 2005).

Electrical cell–substrate impedance sensing

In order to continuously monitor the electrical resistance of cellular monolayers cultured *in vitro* following exposure to industrially relevant ENMs, we utilized electrical cell–substrate impedance sensing (ECIS). Calu-3 cells were seeded onto ECIS 8W10E+ Cultureware Slides (Applied BioPhysics, Inc., Troy, NY) with a growth area of 0.8 cm^2 at a density of 8×10^5 cells per well, and cultured in MEM/5% FBS at 37 °C in humidified air with CO_2. ECIS slides were connected to electrodes on the ECIS Model 1600R (Applied BioPhysics, Inc.), and resistance measurements were collected every 10 min. Once wells reached 2000 Ω, culture media was replaced with ENM suspensions at a concentration of 12.5 μg/ml, and resistance measurements were collected every 10 min for the next 48 h. All experiments were conducted in triplicate.

Immunofluorescence staining

The effect of ENM exposure on cellular tight junctions was also assessed by immunofluorescence staining for intracellular tight junction protein zonula occludens-1 (ZO-1). In brief, following 24-h exposure, transwells were washed in phosphate-buffered saline (PBS), and cells were fixed in 3.7% formaldehyde (MeOH free, J.T. Baker Inc., Phillipsburg, NJ) for 10 min at room temperature. Cells were then washed twice in PBS, and incubated with 50 mM of glycine in PBS for 5 min at room temperature. Fixed cells were permeabilized and blocked with 0.5% saponin/1%BSA/1.5% goat serum for 30 min at room temperature. Rabbit antibody against ZO-1 (Invitrogen, Carlsbad, CA) was diluted 1:100 in 0.5% saponin/1%BSA/1.5% goat serum and incubated with these monolayers at room temperature for 1.5 h. Cells were then incubated with primary antibody (diluted in 0.5% saponin/1%BSA/1.5% goat serum at room temperature for 1.5 h, followed by rinsing three times with 0.5% saponin in PBS at room temperature for 15 min. Monolayers were then incubated with secondary antibody [Alexa Fluor 488 goat anti-rabbit IgG (H + L); Invitrogen, Carlsbad, CA] diluted 1:100 in 0.5% saponin/1%BSA/1.5% goat serum for 1 h at room temperature in the dark, followed by rinsing three times in 0.5% saponin/PBS for

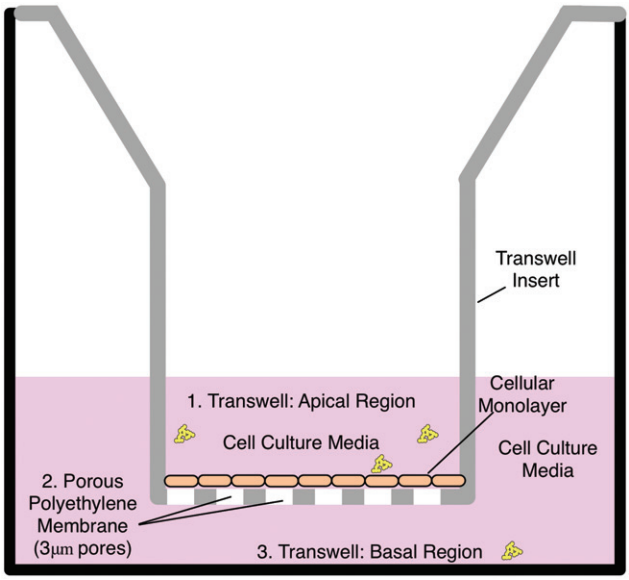

Figure 1. Experimental setup of INVET system.

15 min, and mounted on microscope slides with 20-µl ProLong Gold antifade reagent with 4′,6-diamidino-2-phenylindole (DAPI) (Invitrogen, Carlsbad, CA). Monolayers not exposed to ENMs were similarly incubated with primary and secondary antibodies and processed, serving as negative controls. Images were acquired with a Zeiss Axioplan 200/Axiovert 200 confocal microscope system (Zeiss, Oberkochen, Germany).

INVET system

The experimental setup for tracking translocation of industrially relevant ENMs across cellular monolayers *in vitro* is depicted in Figure 1. 100 µl of ENM suspensions at a concentration of 12.5 µg/ml were applied to both transwells without cells, and transwells with Calu-3 cells cultured to confluence, for 2, 4 and 24 h. The 12.5-µg/ml dose was pre-determined to be below the lethal dose via LDH and MTT cytotoxicity assays (Supplementary Figure 3). Following exposure, all supernatant and transwell inserts were collected from culture plates and set aside for analysis by gamma spectroscopy. All liquid present in the basolateral compartment of the transwell was then collected, and each basal well was washed three times with PBS and collected. Gamma counts were measured for apical compartments (including supernatant and the transwell insert), as well as for the basal compartment (including collected media and PBS wash) by gamma spectroscopy. A mass balance of ENMs measured in the apical and basal compartments was compared to gamma readings for ENM suspensions of equivalent total particle mass (1.25 µg). All experiments were conducted in triplicate.

TEM microscopy

Calu-3 cells were seeded onto 60-mm tissue culture plates with a growth area of 28.0 cm^2 at 2×10^5 cells/plate, and cultured in MEM/5% FBS at 37 °C in humidified air with 5% CO_2. Once cells formed a confluent layer, they were exposed to ENM suspensions at concentration of 12.5 µg/ml. Following 24-h exposure, cells were washed twice in PBS, removed from the culture plate with 0.25% Trypsin (Gibco, Carlsbad, CA), and centrifuged at 1000 *g* for 10 min. Supernatant was decanted, and samples were fixed in Karnovsky's fixative (2.5% glutaraldehyde and 2.5% paraformaldehyde in 0.1 M sodium cacodylate buffer; Electron Microscopy Sciences, Hatfield, PA), then post-fixed in 2% osmium tetroxide (Electron Microscopy Sciences, Hatfield, PA) for 1 h. Samples were then dehydrated and embedded in epon, the blocks were thin sectioned and stained with uranyl acetate and lead citrate (Electron Microscopy Sciences, Hatfield, PA). Images were photographed on a JEOL 1220 transmission electron microscope (Peabody, MA).

Results

Nanomaterial characterization

Properties of ENM powders and dispersions used in this study are summarized in Table 1. Our nanopanel includes CeO_2 ENMs of $d_{XRD} = 28.4$ (CeO_2 small) and $d_{XRD} = 119$ nm (CeO_2 large), ZnO ($d_{XRD} = 28.0$ nm), as well as SiO_2-coated CeO_2 of $d_{XRD} = 28.4$ nm (CeO_2 coated) and SiO_2-coated ZnO of $d_{XRD} = 27.6$ nm (ZnO coated). The variety of properties of the ENM panel allows for parametric comparison of the effects of primary particle size and surface chemistry on ENM translocation across cellular monolayers using the proposed INVET system. Representative electron microscopy images presented in Supplementary Figure 1 illustrate the fractal structure of aggregates, indicative of flame-generated ENMs. In the case of the SiO_2-coated ENMs, a smooth and relatively homogenous 2–4 nm SiO_2-coated layer is visible around the core material (CeO_2 and ZnO, respectively). The hermetic encapsulation of the core ENMs by SiO_2 with minimal effects on the core material has been previously described (Demokritou et al., 2013; Gass et al., 2013).

DLS characterization data presented in Table 1 demonstrates that in general, all ENMs formed agglomerates several times larger than their respective primary particle sizes in both DI H_2O as well as cell culture media, with agglomerate diameters ranging from 200 to 230 nm for all suspensions in MEM/5% FBS. ENM agglomerates were stable for up to 48 h, the duration of our cellular exposures (data not shown), consistent with previous measurements for these materials (Cohen et al., 2012; Gass et al., 2013).

Effect of ENMs on monolayer barrier integrity

As described above and depicted in Figure 1, Calu-3 cell monolayers were cultured on transwell inserts, and monolayer development was monitored by TEER. Monolayer formation was determined when electrical resistance readings measured by TEER exceeded 500 Ω cm^2 (Supplementary Figure 2), consistent with previous reports in the literature (Geys et al., 2006, 2007).

Cellular monolayers with TEER ≥ 500 Ω cm^2 were then exposed to ENMs at an administered dose of 12.5 µg/ml, predetermined to be below the lethal dose via LDH and MTT cytotoxicity assays (Supplementary Figure 4), which is consistent with toxicity results from the literature (Demokritou et al., 2013; Gass et al., 2013; Kroll et al., 2011; Xia et al., 2008a). Figure 2(a) presents TEER readings pre- and post-exposure at each time point, which suggest that ENM exposure did not result in a compromised monolayer and disturbance of tight junctions. Figure 2(b) presents the ECIS resistance measurements taken every 10 min following exposure, providing further support that ENM exposure at 12.5 µg/ml does not compromise tight junctions or monolayer integrity. This data is consistent with previous studies investigating the effect of ZnO particles on cellular monolayers at similar administered mass concentrations (Kim et al., 2010).

Immunofluorescence staining for tight junction protein ZO-1 demonstrated negligible differences between Calu-3 monolayers exposed apically to 25 µg/ml of each ENM suspension for 24 h, compared with cells exposed to particle-free media (Supplementary Figure 5), suggesting ENM exposure leads to negligible disruption of continuity of tight junctions. These

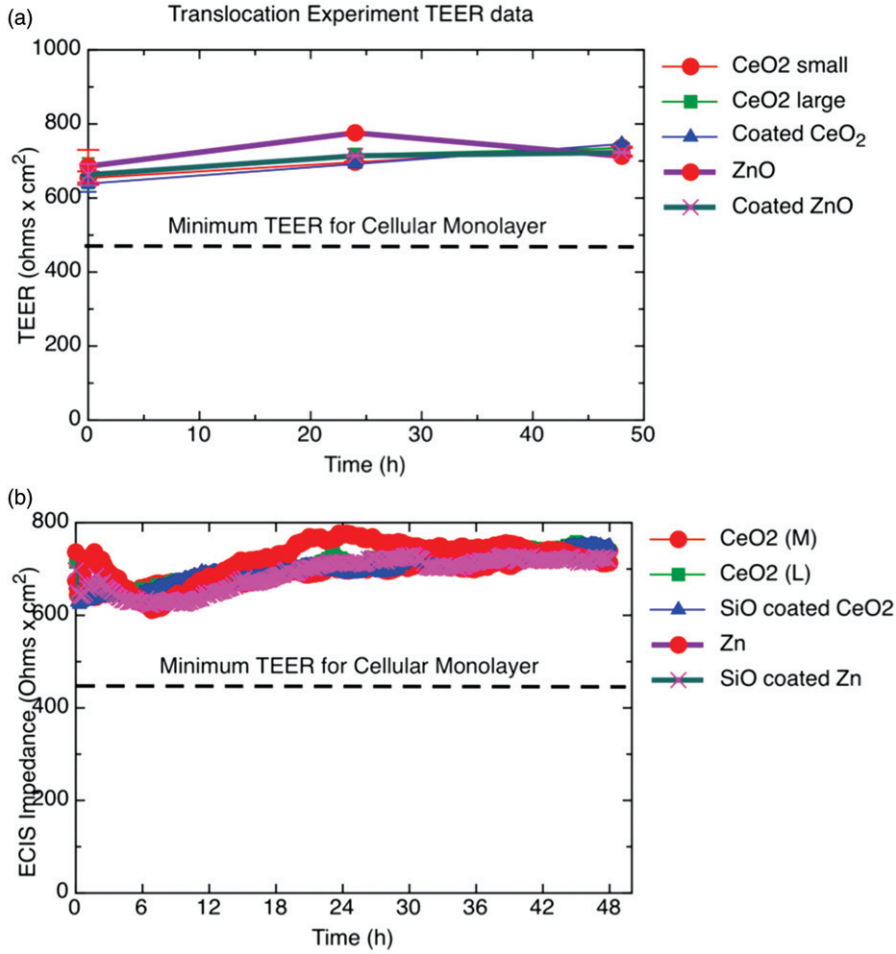

Figure 2. Effect of ENM exposure on monolayer electrical resistance. (a) TEER of Calu-3 monolayers pre- and post-ENM exposure, error bars represent standard deviation and (b) continuous resistance measurements via ECIS during 48-h exposure to ENM suspensions, error bars represent standard deviation.

images are consistent with previously published confocal slices of ZO-1 stains, exhibiting high density of ZO-1 proteins principally at cell borders (Ye et al., 2009). This data further support our TEER and ECIS results, suggesting that ENM exposures at the low concentrations investigated do not compromise Calu-3 monolayer barrier function, nor do they disrupt tight junctions.

Tracking ENM translocation across cellular monolayers

ENM translocation across transwell filter membrane without cells—particle loss assessment

The ability of our ENM agglomerates to successfully pass through the 3-μm pores of the transwell insert membrane in the absence of cells following 24-h incubation was investigated in order to account for potential particle losses within the system. All five ENMs investigated easily permeated through the naked porous filter (<4% of the administered ENMs were collected from the transwell membrane, Supplementary Figure 6). A complete mass balance of administered particles was achieved for all ENMs, where the sum of ENMs measured in each compartment (supernatant, transwell membrane, and basolateral) was equal to the administered dose value, suggesting all ENMs are accounted for in our proposed *in vitro* translocation system (Supplementary Figure 6).

In vitro *dosimetric considerations*

The recently developed methodology to determine the delivered to cell dose was employed for all ENMs investigated (Deloid et al., 2013), whereby ENM deposition *in vitro* via sedimentation and diffusion was estimated based on careful characterization of agglomerate parameters including hydrodynamic diameter and agglomerate effective density. Supplementary Figure 6 reports the estimated delivered to cell dose after 24-h exposure for each material investigated, which in general strongly agreed with the translocated through the membrane dose for each material after 24-h exposure (defined as the sum of ENMs measured on the transwell membrane and in the basolateral compartment), a clear indication of the validity of the proposed *in vitro* dosimetry methodology.

Figure 3 presents the estimated particle deposition curves over time for the three ENMs investigated for translocation across cellular monolayers at various time exposures. Large differences were estimated in the rate of particle delivery to cells across the ENMs studied. For example, after 24-h exposure time, 99% of CeO_2 large is delivered to cells, while only 58% of CeO_2 small is delivered to cells. This discrepancy is largely due to differences in effective density of the two ENMs (2.368 and 1.365 g/cm^3, respectively), which is directly related to sedimentation speed.

ENM translocation across cellular monolayers

Figure 4(a) summarizes the amount of each ENMs detected in the basolateral compartment by gamma spectroscopy after 24-h exposure duration using the INVET systems. These values are reported as both a percentage of the administered dose (Figure 4a), and normalized to the percentage of the delivered to cell dose based on the estimated delivered dose fractions (Figure 4b). Following 24 h of exposure, very low amounts of each ENM were measured in the basolateral compartment (<0.01% administered dose) (Figure 4a). The results from ANOVA indicate the mean values for each ENM are statistically different from each other, though the low values of translocated particles make ranking the translocation potential of all ENMs investigated

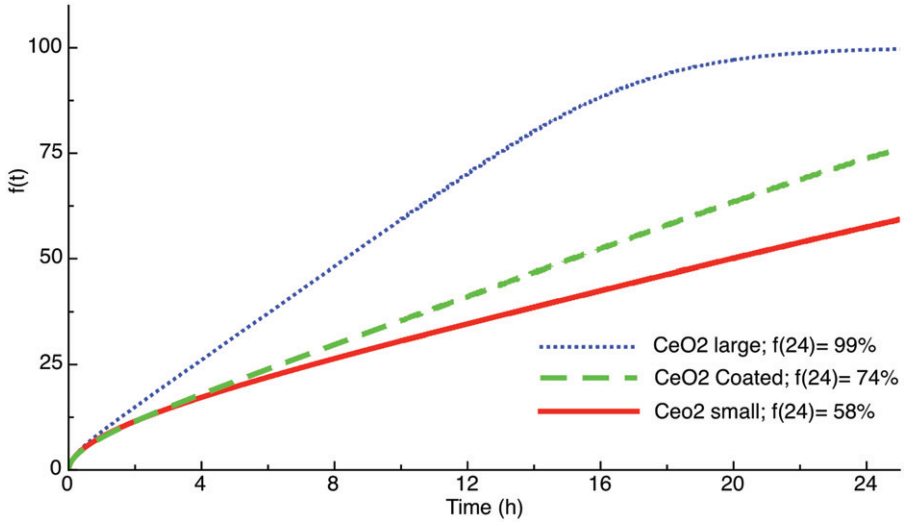

Figure 3. Estimation of particle delivery to cells over 24-h exposure period, f(24): fraction of administered dose delivered to cells following 24-h exposure.

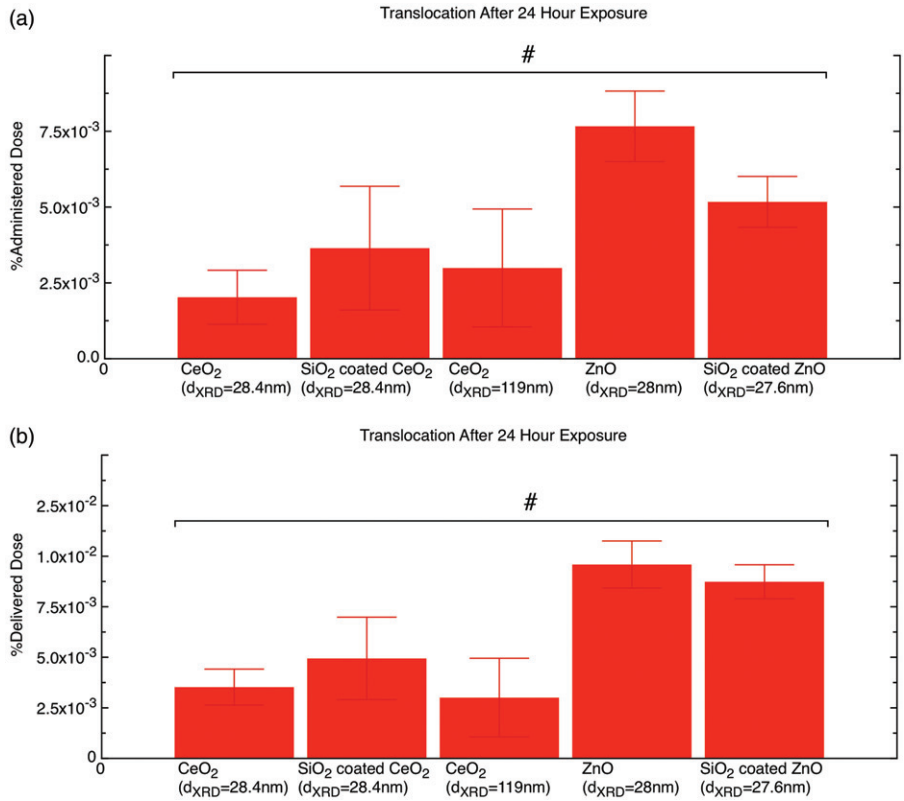

Figure 4. Translocation of ENMs across cellular monolayer *in vitro*. (a) Percent of administered dose measured in basolateral compartment of *in vitro* system following 24-h exposure. (b) Percent of delivered dose for ENMs measured in basolateral compartment following 24-h exposure. All experiments were done in triplicate, error bars represent standard deviation. Hash (#) indicates mean values for each material are not all equal (ANOVA) for $p < 0.05$.

difficult. When dosimetry is taken into consideration, the difference between the two-sized CeO_2 particles ($d_{XRD} = 28.4$ and 119 nm, respectively) is decreased, indicative of the importance of dosimetry *in vitro*. ZnO still exhibits the greatest translocation ability per delivered to cell dose (Figure 4b).

Figure 5 presents time-resolved translocation data for CeO_2 (for both primary particle sizes) and SiO_2-coated CeO_2 after 2, 4 and 24-h exposure. Overall, very small amounts of all three ENMs successfully translocated into the basolateral compartment (<0.01%, Figure 5a). CeO_2 large exhibited slightly greater translocation than CeO_2 small at each time period. Additionally, for all three particles used here, increased translocation associated with increasing exposure duration from 4 to 24 h was observed (e.g. CeO_2 $d_{XRD} = 28.4$ nm: 0.00038% versus 0.0020%). However, when normalized to delivered to cell dose, the amount of CeO_2 small and CeO_2 large measured in the basolateral compartment were found to be are roughly equal, and differences in translocation associated with increased exposure time also disappeared (Figure 5b). For example, after 24-h exposure, the percent of delivered to cell particles (by mass) that translocated across the cellular monolayer for CeO_2 small was 0.0035%, and for CeO_2 large was 0.0030%. It is worth noting that SiO_2-coated CeO_2 exhibited greater translocation than both bare CeO_2 particles even when normalized to the delivered dose (Figure 5b), a clear indication that surface chemistry plays an important role in translocation.

Cellular internalization of ENMs

Electron micrographs of cells exposed to ENMs for 24 h were collected to determine the intracellular localization of ENM particles. Figure 6 presents representative images for Calu-3 cells exposed to CeO_2 large (6a), and CeO_2 small (6b). These images provide qualitative confirmation of cellular internalization,

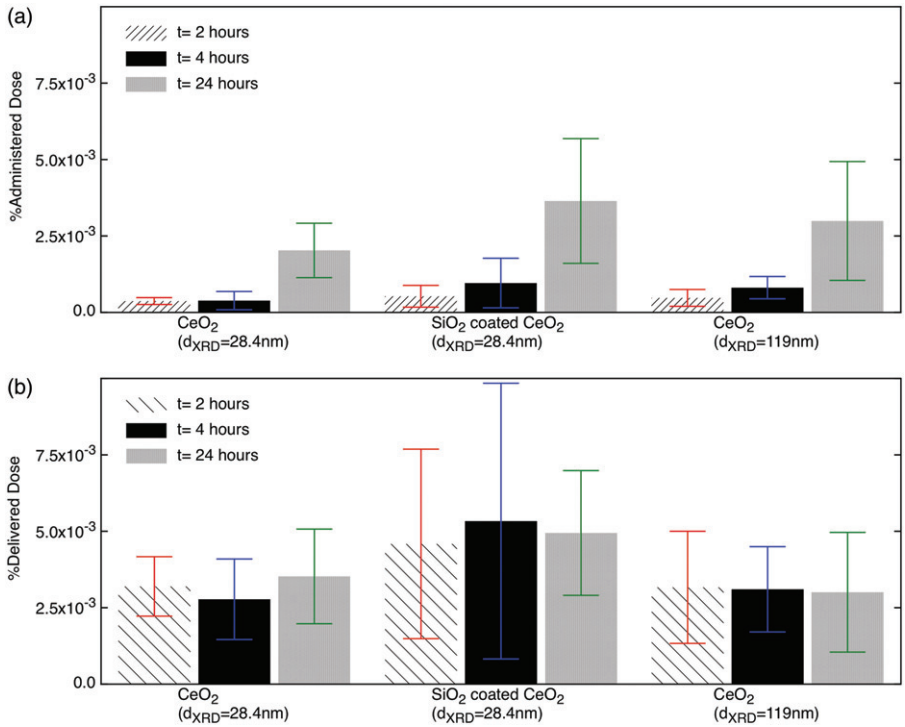

Figure 5. (a) Percent of administered dose for insoluble ENMs measured in basolateral compartment of *in vitro* system following 2, 4 and 24-h exposure. (b) Percent of delivered dose for insoluble ENMs measured in basolateral compartment following 2, 4 and 24-h exposure. All experiments were performed in triplicate. Error bars represent standard deviation.

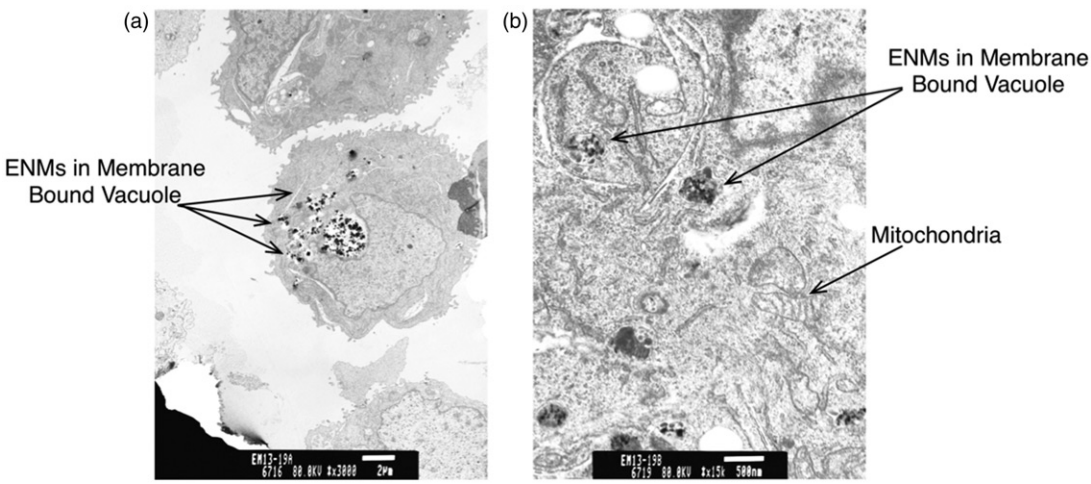

Figure 6. TEM images of ENMs internalized by Calu-3 cells following 24-h exposure. (a) CeO_2 large and (b) CeO_2 small.

evidence that ENMs translocate across cellular monolayers via a predominantly transcellular pathway. In general, CeO_2 ENMs appear encapsulated within membrane-bound vacuoles. There appears to be greater quantities of CeO_2 large particles internalized after 24-h exposure, consistent with the estimated fast deposition rate and high delivered to cell dose estimated for this particle (Figure 3). It is worth noting that ENM aggregates appear concentrated within large endosomal vacuoles (Figure 6a). The CeO_2 small particles appear internalized within later stage endosomal vacuoles, already fused with lysosomes and consolidated with other cellular debris. Similarly, representative images for the other particles provide evidence for cellular internalization and are included in Supplementary Figure 7.

Discussion

Neutron-activated tracer particle system

The data presented here illustrate the high sensitivity of the described radiolabel method which enables rapid and accurate detection of extremely small quantities of ENM in various *in vitro* systems. Furthermore, neutron activation has been shown to induce minimal effects on particle properties (He et al., 2010; Yeh et al., 2012). One limitation of the proposed particle system is the short half-life of some radioisotopes (^{141}Ce, $t_{1/2} = 32$ days), making necessary careful planning and time management of all cellular studies once ENMs have been irradiated.

Calu-3 *in vitro* model of alveolar epithelium

It must be noted that the Calu-3 human epithelial monolayer system used here is a simplified model of the alveolar region, consisting of type II alveolar epithelial cells which only account for <5% of the total surface area of the alveolar wall due to their distinct morphology, and are less likely to come into contact with inhaled ENMs than type I cells (West, 2008). Additionally, the distinct morphology of type II pneumocytes may have implications for particle–cell interactions in terms of the time required for particle endocytosis and exocytosis (West, 2008).

Furthermore, our monoculture model lacks phagocytic macrophages largely responsible for clearance and elimination of

insoluble deposited particles through the tracheobronchial tree toward the larynx (Geiser & Kreyling, 2010; Kreyling et al., 2009; Semmler et al., 2004). It is worth noting that recent studies report non-specific and sporadic phagocytosis of TiO_2 ENMs by alveolar macrophages *in vivo*, suggesting ENMs are able to evade a major clearance mechanism and that there is an increased likelihood for direct interactions with the alveolar epithelium (Geiser et al., 2008). Few nanotoxicology studies have developed 3D triple co-culture systems with primary epithelial cells, along with phagocytic macrophages and dendritic cells to simulate more realistic physiological conditions (Lehmann et al., 2011). Such sophisticated co-culture systems are necessary to improve the physiological relevance of *in vitro* translocation studies (Lehmann et al., 2011; Muller et al., 2011; Rothen-Rutishauser et al., 2005), and should be adopted in future studies to bring more physiological relevance to *in vitro* studies.

Translocation of industrially relevant ENMs using the proposed INVET system

It is clear from the aforementioned data that only small quantities of the ENMs used in this study are able to translocate transcellularly across Calu-3 cells without compromising the monolayer barrier or disrupting tight junctions. Yacobi et al. (2010) recently reported similar findings after exposing rat alveolar epithelial cell monolayers to fluorescently labeled non-agglomerating polystyrene nanoparticles (PNPs). However, PNP's are not industrially relevant particles with high risk of inhalation exposure. The translocation potential of each ENM material used in this study is discussed in more detail below.

CeO_2 ENMs

Both the size- and time-dependent differences in translocation are likely attributable to the differences in the delivered to cell dose of particles at each exposure time point. Limbach (2005) recently reported cellular uptake of CeO_2 ENMs at low exposure concentrations may be limited to particle delivery to cells. Indeed, when normalized to delivered dose, the amount of CeO_2 small and CeO_2 large we measured in the basolateral compartment are roughly equal, and differences in translocation associated with increased exposure time also disappear (Figure 5b). This data supports the theory that ENM–cell interactions *in vitro* largely depend on particle delivery to cells, emphasizing the importance of accurate dosimetry for *in vitro* nanotoxicology.

Our results for CeO_2 are also consistent with previously reported findings indicating that extremely small quantities of CeO_2 are able to translocate across a cellular monolayer quickly *in vivo*, with only small increases in total flux at longer exposure durations. A recent study investigating the biodistribution of CeO_2 instilled in the lungs of Wistar rats reported small quantities of CeO_2 nanoparticles are capable of quickly accessing the bloodstream and entering transpulmonary organs within 10 min post-exposure, though the majority of particles are persistent in the lungs weeks after instillation (64% of instilled particles remained in the lung at 28 days post-exposure) (He et al., 2010). It is clear that CeO_2 ENMs are able to translocate across cellular monolayers both *in vitro* and *in vivo* at extremely low levels, and translocation likely occurs via transcellular pathways.

SiO_2-coated ENMs

Both SiO_2-coated CeO_2 and SiO_2-coated ZnO ENMs exhibited greater translocation than both bare CeO_2 ENMs at 24-h exposure (Figure 4a). SiO_2-coated CeO_2 exhibited greater translocation than bare CeO_2 even when normalized to the delivered dose (Figure 4b), suggesting surface chemistry plays a significant role in ENM translocation across cellular monolayers. Increases in translocation associated with increasing exposure time (2, 4 and 24 h) disappear when normalized to delivered dose (Figure 5), supporting the theory that ENM–cellular interactions are greatly influenced by particle delivery to cells and emphasizing the importance of dosimetry considerations for *in vitro* nanotoxicology.

Our findings for both SiO_2-coated ENMs are consistent with recently reported *in vivo* investigations reporting translocation of pure SiO_2 particles. Amorphous SiO_2 ENMs of various primary particle size were instilled in the lungs of Wistar rats at relatively high doses (2, 5 and 10 mg/kg by weight), and exhibited the ability to pass through the alveolar epithelium into systemic circulation and induce cardiovascular toxicity (Du et al., 2013). However, the exceedingly high doses used in this study may have resulted in lung particle overload and impaired alveolar macrophage-mediated particle clearance, leading to increased particle accumulation in the lungs and increased potential for lung injury, compromise of the air–blood barrier and increased translocation events to occur (Oberdorster, 1995). In spite of this limitation, our results support the growing body-of-evidence that amorphous SiO_2 particles and SiO_2-coated ENMs are capable of translocation across the alveolar epithelium into the systemic circulation via transcellular pathways.

ZnO ENMs

ZnO exhibited the greatest amount of translocation following 24-h exposure (Figure 4a). It is important to note that the measured translocation for ZnO ENMs does not distinguish between ZnO particles and Zn^{2+} ions associated with partial solubility of the ZnO. While Zhang et al. (2012) recently reported 35% dissolution of ZnO ENMs following 24-h incubation in cell culture media, time-resolved solubility studies for this material will be required to determine the dissolution rate over time in cell culture media to further elucidate this issue. Significantly, ZnO particles of agglomerate diameter 230 nm were measured by DLS in the basolateral media, providing evidence of particle translocation following 24-h exposure. Future studies are required to further distinguish the translocation kinetics of particulate ZnO versus translocation of zinc ions.

Cellular internalization of ENMs

While our study provides some insight into understanding ENM translocation across epithelial barriers, more work is necessary to determine the mechanisms of cellular internalization. Several groups report a relationship between ENM properties (diameter, surface charge, etc.) and endocytic mechansims, though often with conflicting results (Nel et al., 2009). For example, Chithrani et al. (2006) reported an optimal diameter of 200 nm for clathrin-mediated uptake, and 500 nm for caveolin-mediated uptake. In contrast, Gratton et al. (2008) report the optimal diameter ranges from 50-80 nm for clathrin-mediated uptake, and is 120 nm for caveolin-mediated uptake. With regards to particle translocation, Yacobi et al. (2010) reported higher translocation rates for amidine-modified PNPs compared with carboxylate-modified PNPs, suggesting that direct interactions between PNPs and cell membranes may be the predominant mechanism for PNP internalization and translocation across primary rat alveolar epithelial cell monolayers.

It is clear that additional *in vitro* and *in vivo* studies are necessary to further elucidate the specific endocytic and exocytic mechanisms underlying translocation of industrially relevant ENMs, and our group is currently working to investigate these issues utilizing the developed INVET platform.

Conclusions

In this study, we present a novel *in vitro* model for tracking the translocation of industrially relevant metal oxide ENMs across cellular monolayers *in vitro*. While neutron-activated industrially relevant ENMs have been used for biodistribution studies *in vivo*, this is the first time such an approach has been used *in vitro* to assess particle–cell interactions. With the ever-increasing number and variety of ENMs entering the consumer market, efficient and inexpensive *in vitro* models such as the one presented here are needed to correlate ENM properties with biological activity. The versatility and high sensitivity of this approach was demonstrated using a panel of industrially relevant ENMs of variable size and chemical composition and surface chemistry. We report that CeO_2 of various primary particle sizes, ZnO, SiO_2-coated CeO_2 and SiO_2-coated ZnO ENMs are able to translocate transcellularly across Calu-3 cellular monolayers at low doses, without compromising the alveolar epithelial barrier integrity, nor disrupting tight junctions at cell–cell borders. Electron micrographs of exposed cells exhibiting ENMs internalized by cells localized near large endosomal vacuoles provide supporting evidence that the translocation pathway is transcellular rather paracellular.

Currently, there is indirect validation of our *in vitro* results published in the literature for each material based on instillation experiments *in vivo*. Additionally, our group is currently preparing manuscripts summarizing the results of *in vivo* pharmacokinetic studies investigating translocation of the particular materials used in our INVET system and reported on here. Though it was observed that very few particles were able to translocate across healthy cellular monolayers, the kinetics and mechanisms of ENM translocation may be different for unhealthy monolayers with disrupted tight junctions. For example, ozone exposure is known to increase the permeability of the air–blood barrier, with implications for increased translocation of ENM particles. Furthermore, the results of this study highlight the importance of dosimetry for accurate *in vitro* nanotoxicity studies. Although additional *in vitro* and *in vivo* studies are required to further elucidate the specific endocytic and exocytic mechanisms underlying ENM translocation at physiologically relevant exposure doses, it is clear that industrially relevant metal oxide ENMs are capable of crossing healthy alveolar monolayers without compromising the epithelium barrier integrity.

Declaration of interest

The authors report no conflicts of interest. The authors alone are responsible for the content and writing of this article. The findings and conclusions in this article are those of the authors and do not necessarily represent the views of the National Institute for Occupational Safety and Health.

This research project was supported by NIEHS grant (ES-0000002), NSF grant (ID 1235806) and the Center for Nanotechnology and Nanotoxicology at The Harvard School of Public Health.

References

Aitken RC, Chaudhry MQ, Boxall AB, Hull M. 2006. Manufacture and use of nanomaterials: current status in the UK and global trends. Occup Med 56:300–6.

Bello D, Martin J, Santeufemio C, Sun Q, Lee Bunker K, Shafer M, Demokritou P. 2012. Physicochemical and morphological characterisation of nanoparticles from photocopiers: implications for environmental health. Nanotoxicology 7:989–1003.

Brain J. 2009. Biologic responses to nanomaterials depend on exposure, clearance, and material characteristics. Nanotoxicology 3:1–7.

Chen JK, Shih MH, Pier JJ, Liue CH, Chou FI, Lai WH, et al. 2010. The use of radioactive zinc oxide nanoparticles in determination of their tissue concentrations following intravenous administration in mice. Analyst 135:1742–6.

Chithrani BD, Ghazani AA, Chan WCW. 2006. Determining the size and shape dependence of gold nanoparticle uptake into mammalian cells. Nano Lett 6:662–8.

Choi HS, Ashitate Y, Lee JH, Kim SH, Matsui A, Insin N, et al. 2010. Rapid translocation of nanoparticles from the lung airspaces to the body. Nat Biotechnol 28:1300–3.

Cohen J, Deloid G, Pyrgiotakis G, Demokritou P. 2012. Interactions of engineered nanomaterials in physiological media and implications for *in vitro* dosimetry. Nanotoxicology 7:417–31.

Conner SD, Schmid SL. 2003. Regulated portals of entry into the cell. Nature 422:37–44.

Deloid G, Cohen JM, Darrah T, Derk R, Rojanasakul L, Pyrgiotakis G, et al. 2013. Estimating effective density of engineered nanomaterials for *in vitro* dosimetry. Nat Commun.

Demokritou P, Buchel R, Molina RM, Deloid GM, Brain JD, Pratsinis SE. 2010. Development and characterization of a Versatile Engineered Nanomaterial Generation System (VENGES) suitable for toxicological studies. Inhal Toxicol 22(Suppl. 2):107–16.

Demokritou P, Cohen JM, Deloid G. 2012. Novel methods of measuring effective density of nanoparticles in fluids. US Provisional Patent Application No. 61/661,895.

Demokritou P, Gass S, Pyrgiotakis G, Cohen JM, Goldsmith W, Mckinney W, et al. 2013. An *in vivo* and *in vitro* toxicological characterization of realistic nanoscale CeO_2 inhalation exposures. Nanotoxicology 7:1338–50.

Du Z, Zhao D, Jing L, Cui G, Jin M, Li Y, et al. 2013. Cardiovascular toxicity of different sizes amorphous silica nanoparticles in rats after intratracheal instillation. Cardiovasc Toxicol 13:194–207.

Gass S, Cohen JM, Pyrgiotakis G, Sotiriou GA, Buechel R, Pratsinis SE, Demokritou P. 2013. A safer formulation concept for flame-generated engineered nanomaterials. ACS Sustain Chem Eng 1:843–57.

Geiser M, Casaulta M, Kupferschmid B, Schulz H, Semmler-Behnke M, Kreyling W. 2008. The role of macrophages in the clearance of inhaled ultrafine titanium dioxide particles. Am J Respir Cell Mol Biol 38: 371–6.

Geiser M, Kreyling WG. 2010. Deposition and biokinetics of inhaled nanoparticles. Part Fibre Toxicol 7:2.

Geiser M, Rothen-Rutishauser B, Kapp N, Schurch S, Kreyling W, Schulz H, et al. 2005. Ultrafine particles cross cellular membranes by nonphagocytic mechanisms in lungs and in cultured cells. Environ Health Perspect 113:1555–60.

Geys J, Coenegrachts L, Vercammen J, Engelborghs Y, Nemmar A, Nemery B, Hoet PH. 2006. *In vitro* study of the pulmonary translocation of nanoparticles: a preliminary study. Toxicol Lett 160: 218–26.

Geys J, Nemery B, Hoet PH. 2007. Optimisation of culture conditions to develop an *in vitro* pulmonary permeability model. Toxicol In Vitro 21: 1215–19.

Gratton SEA, Roop PA, Pohihaus PD, Luft JC, Madden VJ, Napier ME, Desimone JM. 2008. The effect of particle design on cellular internalization pathways. Proc Natl Acad Sci USA 105:11613–18.

Haynes WM. 2012. CRC Handbook of Chemistry and Physics, 92nd edn. Boca Raton (FL): CRC Press.

He X, Zhang H, Ma Y, Bai W, Zhang Z, Lu K, et al. 2010. Lung deposition and extrapulmonary translocation of nano-ceria after intratracheal instillation. Nanotechnology 21:285103–11.

Hinderliter PM, Minard KR, Orr G, Chrisler WB, Thrall BD, Pounds JG, Teeguarden JG. 2010. ISDD: a computational model of particle sedimentation, diffusion and target cell dosimetry for *in vitro* toxicity studies. Part Fibre Toxicol 7:36.

Kim KJ, Crandall ED. 1983. Heteropore populations of bullfrog alveolar epithelium. J Appl Physiol 54:140–6.

Kim YH, Fazlollahi F, Kennedy IM, Yacobi NR, Hamm-Alvarez SF, Borok ZEA, et al. 2010. Alveolar epithelial cell injury due to zinc oxide nanoparticle exposure. Am J Respir Crit Care Med 182: 1398–409.

Kreyling WG, Semmler-Behnke M, Seitz J, Scymczak W, Wenk A, Mayer P, et al. 2009. Size dependence of the translocation of inhaled iridium and carbon nanoparticle aggregates from the lung of rats to the blood and secondary target organs. Inhal Toxicol 21(Suppl. 1):55–60.

Kroll A, Dierker C, Rommel C, Hahn D, Wohlleben W, Schulze-Isfort C, et al. 2011. Cytotoxicity screening of 23 engineered nanomaterials using a test matrix of ten cell lines and three different assays. Part Fibre Toxicol 8:9.

Lehmann AD, Daum N, Bur M, Lehr CM, Gehr P, Rothen-Rutishauser BM. 2011. An *in vitro* triple cell co-culture model with primary cells mimicking the human alveolar epithelial barrier. Eur J Pharm Biopharm 77:398–406.

Limbach L. 2005. Oxide nanoparticle uptake in human lung fibroblasts: effects of particle size, agglomeration, and diffusion at low concentrations. Environ Sci Technol 39:9370–6.

Matsukawa Y, Lee VH, Crandall ED, Kim KJ. 1997. Size-dependent dextran transport across rat alveolar epithelial cell monolayers. J Pharm Sci 86:305–9.

Mills NL, Donaldson K, Hadoke PW, Boon NA, Macnee W, Cassee FR, et al. 2009. Adverse cardiovascular effects of air pollution. Nat Clin Pract Cardiovasc Med 6:36–44.

Muller LG, Gasser M, Raemy DO, Herzog F, Brandenberger C, Schmid O, et al. 2011. Realistic exposure methods for investigating the interaction of nanoparticles with the lung at the air-liquid interface *in vitro*. Insciences J 1:30–64.

Nel AE, Madler L, Velegol D, Xia T, Hoek EM, Somasundaran P, et al. 2009. Understanding biophysicochemical interactions at the nano-bio interface. Nat Mater 8:543–57.

Oberdorster G. 1995. Lung particle overload: implications for occupational exposures to particles. Regul Toxicol Pharmacol 21:123–35.

Pirela S, Molina R, Watson C, Cohen JM, Bello D, Demokritou P, Brain J. 2013. Effects of copy center particles on the lungs: a toxicological characterization using a Balb/c mouse model. Inhal Toxicol 25: 498–508.

Rothen-Rutishauser BM, Kiama SG, Gehr P. 2005. A three-dimensional cellular model of the human respiratory tract to study the interaction with particles. Am J Respir Cell Mol Biol 32:281–9.

Semmler M, Seitz J, Erbe F, Mayer P, Heyder J, Oberdorster G, Kreyling WG. 2004. Long-term clearance kinetics of inhaled ultrafine insoluble iridium particles from the rat lung, including transient translocation into secondary organs. Inhal Toxicol 16:453–9.

Sotiriou GA, Diaz E, Long MS, Godleski J, Brain J, Pratsinis SE, Demokritou P. 2011. A novel platform for pulmonary and cardiovascular toxicological characterization of inhaled engineered nanomaterials. Nanotoxicology 11:680–90.

Sotiriou GA, Franco D, Poulikakos D, Ferrari A. 2012. Optically stable biocompatible flame-made SiO_2-coated Y2O3: Tb3+ nanophosphors for cell imaging. ACS Nano 6:680–90.

Teeguarden JG, Hinderliter PM, Orr G, Thrall BD, Pounds JG. 2007. Particokinetics *in vitro*: dosimetry considerations for *in vitro* nanoparticle toxicity assessments. Toxicol Sci 95:300–12.

Tenuta T, Monopoli MP, Kim J, Salvati A, Dawson KA, Sandin P, Lynch I. 2011. Elution of labile fluorescent dye from nanoparticles during biological use. PLoS One 6:e25556.

Wang B, Wang Z, Feng W, Wang M, Hu Z, Chai Z, Zhao Y. 2010. New methods for nanotoxicology: synchrotron radiation-based techniques. Anal Bioanal Chem 398:667–76.

Wegner KP, Pratsinis SE. 2003. Scale-up of nanoparticle synthesis in diffusion flame reactors. Chem Eng Sci 58:4581–9.

West JB. 2008. Respiratory Physiology: the Essentials. Philadelphia (PA): Lippincott Williams & Wilkins.

Xia T, Kovochich M, Liong M, Madler L, Gilbert B, Shi H, et al. 2008a. Comparison of the mechanism of toxicity of zinc oxide and cerium oxide nanoparticles based on dissolution and oxidative stress properties. ACS Nano 2:2121–34.

Xia T, Kovochich M, Liong M, Zink JI, Nel AE. 2008b. Cationic polystyrene nanosphere toxicity depends on cell-specific endocytic and mitochondrial injury pathways. ACS Nano 2:85–96.

Yacobi NR, Malmstadt N, Fazlollahi F, Demaio L, Marchelletta R, Hamm-Alvarez SF, et al. 2010. Mechanisms of alveolar epithelial translocation of a defined population of nanoparticles. Am J Respir Cell Mol Biol 42:604–14.

Yang S, Song C, Qiu T, Guo L, Li X. 2013. Synthesis of polystyrene/polysilsesquioxane core/shell composite particles via emulsion polymerization in the existence of poly(gamma-methacryloxypropyl trimethoxysilane) sol. Langmuir 29:92–101.

Ye P, Nadkarni MA, Simonian M, Hunter N. 2009. CD24 regulated gene expression and distribution of tight junction proteins is associated with altered barrier function in oral epithelial monolayers. BMC Cell Biol 10:2.

Yeh TK, Chen JK, Lin CH, Yang MH, Yang CS, Chou FI, et al. 2012. Kinetics and tissue distribution of neutron-activated zinc oxide nanoparticles and zinc nitrate in mice: effects of size and particulate nature. Nanotechnology 23:085102–085111.

Zhang H, Ji Z, Xia T, Meng H, Low-Kam C, Liu R, et al. 2012. Use of metal oxide nanoparticle band gap to develop a predictive paradigm for oxidative stress and acute pulmonary inflammation. ACS Nano 6: 4349–68.

Supplementary material available online

Supplementary Figures 1–7